Supporting information for:

Plasma-Driven Electrocatalytic Ammonia Synthesis: A Pulsed NO_x Replenishment Strategy

Chenxi Man[1, 3, a], Zhiyuan Xu[2, 3, a], Bingtao Xie[3, 4], Shuai Zhang[3, 4], Bangdou Huang[3, 4], Dengke Xi[3], Xuekai Pei[1], Leslie Petrik[5], Cheng Zhang[3, 4. *], Tao Shao[1, 3, 4 *]

1 State Key Laboratory of Power Grid Environmental Protection (School of Electrical Engineering and Automation), Wuhan University, Wuhan 430072, China

2 Institute of Next Generation Power Systems & International Standards, Wuhan University, Wuhan 430072, China

3 Beijing International S&T Cooperation Base for Plasma Science and Energy Conversion, Institute of Electrical Engineering, Chinese Academy of Sciences, Beijing 100190, China

4 University of Chinese Academy of Sciences, Beijing 100049, China

5 Environmental and Nano Sciences Group, Department of Chemistry, University of the Western Cape, Bellville, Cape Town 7535, Republic of South Africa

Corresponding author:

Cheng Zhang (zhangcheng@mail.iee.ac.cn) and Tao Shao (shaotao@whu.edu.cn)

[a] These authors contributed equally to this work.

1.1 characterizations

X-ray diffraction (XRD, D8 Advance, Bruke) was employed to characterize the crystalline structure of the catalyst, and X-ray photoelectron spectroscopy (XPS, KAlpha, Thermo Fisher Scientific) was utilized for the analysis of the catalyst's chemical composition and elemental valence states. High-resolution transmission electron microscopy (HRTEM, JEM-2010, JEOL) provided insights into the internal structure of the catalytic crystals, , while the scanning electron microscopy (SEM, Supra 55, Zeiss) was used to observe the catalyst morphology. UV-vis spectrophotometer (UV3500s, Lincylab) was employed for the quantification of concentrations of NO_x^- and ammonia in the liquid phase. Voltage and current were monitored using a high-voltage probe (PVM-1, divider ratio 2000:1, NorthStar) and a current probe (6595, divider ratio 0.5 V/A, Pearson), respectively, and recorded with an oscilloscope (DPO2024B, Tektronix).

1.2 Electrochemical tests

All electrochemical tests were conducted within an H-type electrolysis cell (C007 Interchangeable membrane H-type electrolytic cell, Gaossunion) separated by a Nafion 117 ionic exchange membrane, powered by an electrochemical workstation (CHI 760E, Chenhua). The electrolyte consisted of 1 M KOH solution, with 50 mL for both cathode and anode chambers. The gaseous NO_x generated by plasma nitrogen fixation were exclusively bubbled into the cathode chamber to produce the NO_x reactants. The prepared catalyst (with an active reaction area of 1×1 cm), along with a Hg/HgO electrode and a platinum sheet electrode, served as the working, reference, and counter electrodes, respectively, in the three-electrode system. Potentials were converted to the reversible hydrogen electrode (RHE) scale using the Nernst equation:[1]

$$E_{RHE}=E_{Hg/HgO}+0.098+0.0591\times pH \quad (1)$$

1.3 Determination of Ammonia

Nessler's reagent colorimetric method was employed for the quantitative determination of ammonium ion concentrations in the liquid phase. A 5 mL aliquot of the test solution was sampled and diluted. To this, 0.1 mL of potassium sodium tartrate solution and 0.1 mL of Nessler's reagent were added sequentially. The colorimetric reaction was allowed to proceed after the addition of Nessler's reagent. Upon mixing, the ammonium ion (NH_4^+) in the test solution reacted with the reagent to form a yellow-colored complex. The color intensity, which correlates with the concentration of ammonium ions, was developed after a 10-minute incubation period. The absorbance of the resulting solution was then measured at 420 nm using a UV-vis spectrophotometer, with the intensity of the color directly proportional to the NH_4^+ concentration in the liquid phase. Ammonia yield can be calculated by Equation 2:

$$\text{Ammonia Yield} = \Delta C \times V/t \times S \tag{2}$$

Where ΔC is the difference in ammonia concentration before and after the reaction, V is the volume of the cathodic reaction electrolyte (50 mL), t is the reaction time, S is the actual reaction area of catalyst (1 cm^{-2}).

NO_2^- and NO_3^- participated as reactants in the reaction. The concentrations of NO_2^- and NO_3^- before and after the reaction were measured, allowing for the calculation of the average number of transferred electrons (Q_t) by Equation 3:

$$Q_t = 6 \times \Delta C_{NO_2^-} \Big/ (\Delta C_{NO_2^-} + \Delta C_{NO_3^-}) + 8 \times \Delta C_{NO_3^-} \Big/ (\Delta C_{NO_2^-} + \Delta C_{NO_3^-}) \tag{3}$$

Faradaic efficiency can be calculated by Equation 4:

$$FE = (Q_t \times F \times \Delta C \times V)/Q \tag{4}$$

Where Q is the total charge transferred during the electrocatalytic reaction, F is the Faradaic constant (96485 C mol^{-1}).[2, 3]

1.4 Determination of Nitrite

The Sulfanilamide-Naphthyl Ethylenediamine Hydrochloride Colorimetric Method was employed for the determination of nitrite concentration. First, 5 g sulfanilamide was dissolved in 50 mL concentrated hydrochloric acid and 300mL of deionized water, and the resulting sulfanilamide solution was then diluted to 500 mL using deionized water. Separately, 0.5 g of N-(1-naphthyl) ethylenediamine dihydrochloride was dissolved in 500 mL of deionized water to obtain the N-(1-naphthyl) ethylenediamine dihydrochloride solution. A 5 mL aliquot of the test solution was sampled and diluted, then 0.1 mL of sulfanilamide solution and 0.1 mL of N-(1-naphthyl) ethylenediamine dihydrochloride solution were added sequentially at 5-minute intervals. After a 15-minute reaction, the absorbance was measured at 540 nm using a UV-vis spectrophotometer.

1.5 Determination of Nitrate

A 10 mL aliquot of the test solution was sampled and diluted, followed by the addition of 0.1 mL of 6 M HCl. The absorbance was measured using a UV-vis spectrophotometer at wavelengths of 220 nm and 275 nm. To eliminate interference, the absorbance at 275 nm was subtracted from that at 220 nm.[3]

1.6 Energy efficiency

The energy efficiency was calculated using the following formula:

$$\eta_e = \frac{n_{NH_3} \times \Delta H_{NH_3}}{P_{plasma} + P_{electrolysis}}$$

Where n_{NH_3} is the molar formation rate, ΔH_{NH_3} (46 kJ mol^{-1}) is the enthalpy of formation, and P_{plasma} and $P_{electrolysis}$ are the respective electrical inputs. Based on our measured parameters, $\eta_e \approx 17.6\%$, indicating an energetically favorable process relative to continuous plasma–electrolysis operation (typically<10%).

1.7 Energy efficiency

Figure s1 (A) depicts the electrolytic cell employed in this study. Following oxidation of air via a rotating gliding arc, NO_x is introduced into this electrolytic cell. This electrolytic cell employs a three-electrode configuration, with the cathode and anode compartments separated by a hydrogen ion exchange membrane. During operation, the cathode compartment undergoes a reduction reaction, progressively converting NO_x into NH_3. Concurrently, the anode compartment undergoes an oxidation reaction, converting hydroxide ions in the electrolyte (1 M KOH) into oxygen gas. Figure s1 (A) depicts a cross-sectional view of the rotating gliding arc reactor. The central triangular cone serves as the high-voltage electrode (anode), encased by a stainless steel cylinder forming the ground electrode. Upon application of a high-voltage alternating current signal, breakdown occurs first at the shortest distance between the triangular cone electrode and the ground electrode, subsequently gliding down the cone to form a gliding arc. This discharge exhibits glow-like arc characteristics. Spectral fitting of the gas temperature indicates a range of 1400 K-2200 K, corresponding to a non-thermal equilibrium plasma state. Plasma formation occurs exclusively within the reactor depicted in Figure s1 (B). The resulting NO_x gases are subsequently introduced into the electrolytic cell shown in Figure s1 (A) for in situ absorption and reduction.

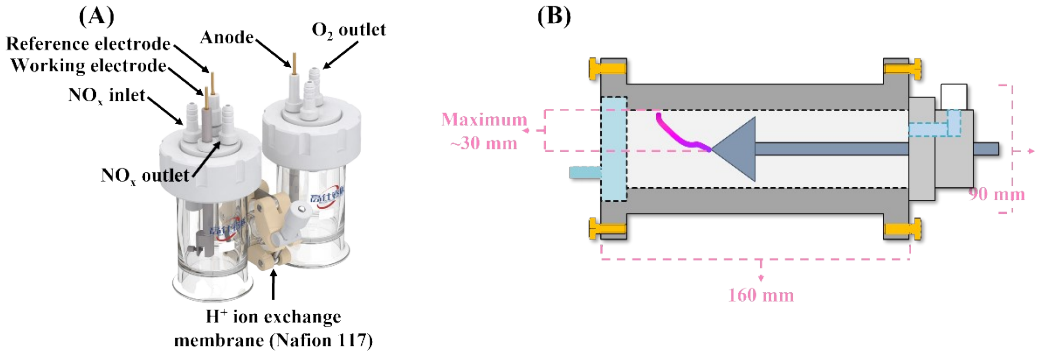

Figure s1. (A) Details of H-cell for electrocatalytic ammonia synthesis, and (B) Rotating gliding arc plasma reactor dimensions.

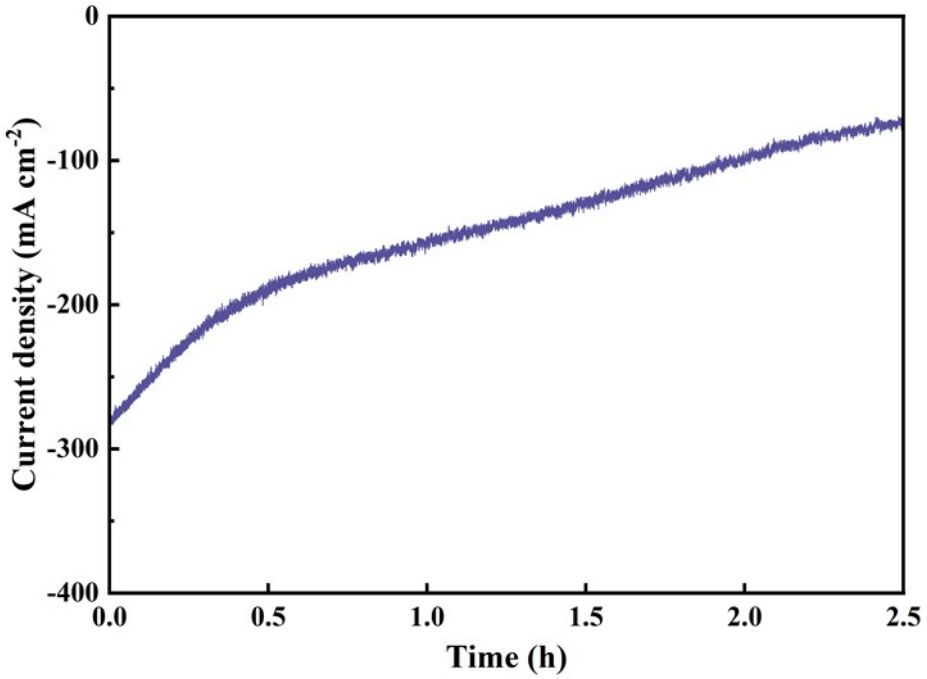

Figure s2. The i-t curve for a single electrocatalytic reaction process.

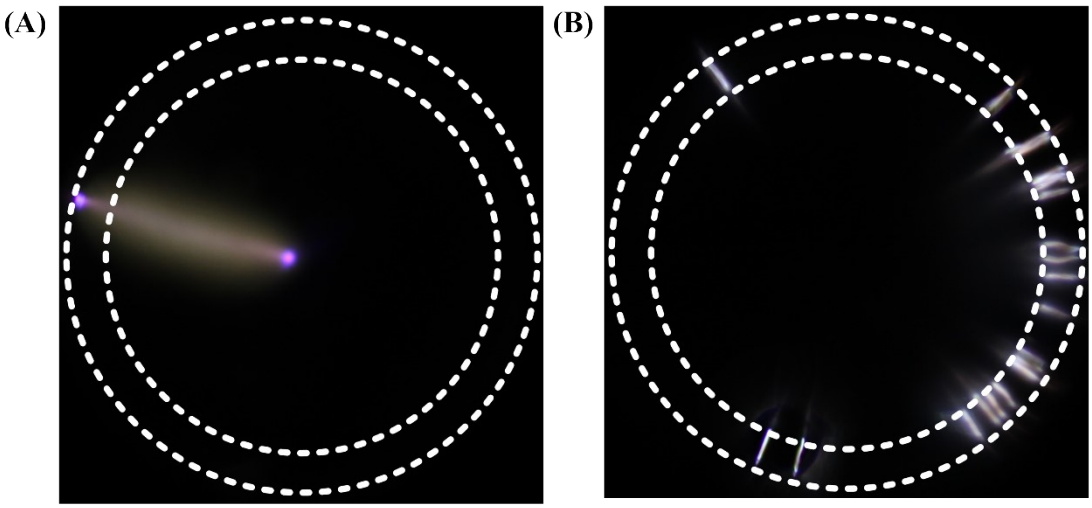

Figure s3. The AC-powered gliding arc discharge exhibited two distinct discharge modes: (A) A-G mode, and (B) B-G mode.

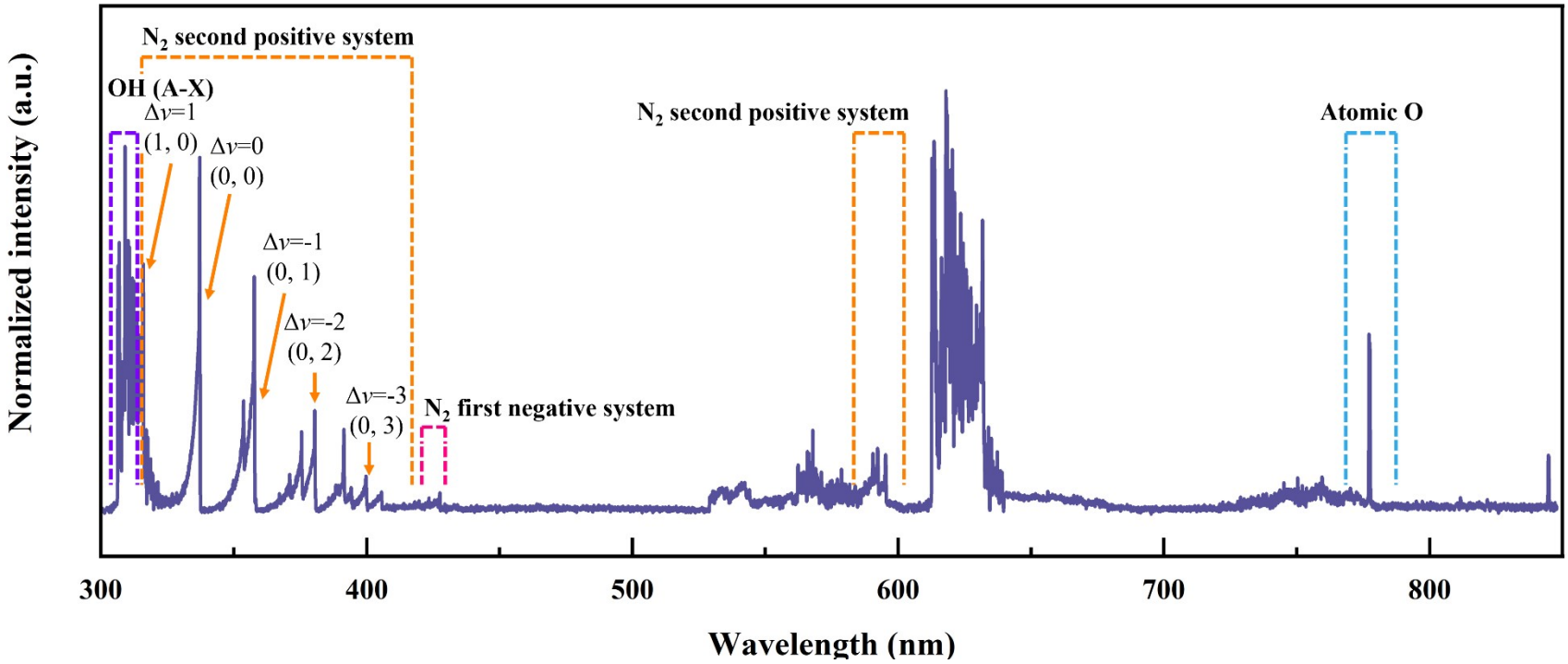

Figure s4. Optical emission spectrum of the air rotating gliding arc.

1.8 Model assumptions and settings

1. Model type and purpose: We used a zero-dimensional global plasma kinetics model (ZDPlaskin) intended to capture the temporal trends and relative dominance of gas-phase reactive nitrogen/oxygen species (RNS/ROS) generated in the discharge. The model is not designed to predict absolute species fluxes at the electrolyte interface, but rather to identify which RNS (e.g., NO, NO_2, N_2O_5) are produced under the experimental reduced field and to compare relative time-evolution under different discharge conditions.

2. Gas composition and pressure: Calculations assume synthetic air composition (78% N_2, 21% O_2, balance inert) at 1 atm.

3. Temperature: The gas temperature is held constant at 2164 K throughout each simulation. Temperature-dependent chemistry (i.e., thermal dissociation reactions) beyond that implicit in rate coefficients evaluated at the chosen temperature is not explicitly coupled to a time-varying gas temperature. We selected 2164 K as representative of our experimental gas-phase conditions (near-ambient with limited heating due to the pulsed operation).

4. Electric field / EEDF: The reduced electric field was set to 97 Td, corresponding to the experimentally used AC field intensity. The electron energy distribution function (EEDF) was approximated under steady-state conditions for that reduced field and used to compute electron-impact rate coefficients for ionization, dissociation, and excitation processes in the reaction set.

5. Reaction set and tracked species: The model includes a comprehensive set of gas-phase electron-impact and heavy-particle reactions relevant to air plasmas, tracking species such as N_2, O_2, N, O, NO, NO_2, N_2O, NO_3, N_2O_5, O_3, electrons, and key ions. Reaction rate coefficients were taken from the standard plasma kinetics literature and databases (references provided in Supporting Information).

Table S1. Important reaction equations and reaction coefficient in gas phase Air plasma model.

Index	Reaction equation	Reaction rate coefficient	Ref.
R01	$e^{-}+N_2 \rightarrow e+N_2(V_i, i=1\text{-}8)$	*f(E/N)*	4
R02	$e^{-}+O_2 \rightarrow e+O_2(V_i, i=1\text{-}4)$	*f(E/N)*	5
R03	$e^{-}+N_2 \rightarrow e+N_2(A3)$	*f(E/N)*	4
R04	$e^{-}+N_2 \rightarrow e+N_2(B3, W3, B'3)$	*f(E/N)*	4
R05	$e^{-}+N_2 \rightarrow e+N_2(a'1, a1, w1)$	*f(E/N)*	4
R06	$e^{-}+N_2 \rightarrow e+N_2(C3, E3, a''1)$	*f(E/N)*	4
R07	$e^{-}+O_2 \rightarrow e^{-}+O_2(a1)$	*f(E/N)*	6
R08	$e^{-}+O_2 \rightarrow e^{-}+O_2(b1)$	*f(E/N)*	6
R09	$e^{-}+N \rightarrow e^{-}+ N(2D)$	*f(E/N)*	6
R10	$N+O_2 \rightarrow O+NO$	$3.2\times10^{-12}(T_g/300)\exp(-3150/T_g)$	7
R11	$NO_2+NO_2 \rightarrow NO+NO_3$	$4.5\times10^{-10}\exp(-18500/T_g)$	8

R12	$NO_2+NO \rightarrow NO+O+NO$	$5.304\times10^{-5}(300/T_g)^2\exp(-36180/T_g)$	8
R13	$NO_3+N2 \rightarrow NO+O_2+N_2$	$6.2\times10^{-5}(300/T_g)^2\exp(-25000/T_g)$	8
R14	$O+NO+NO \rightarrow NO_2+NO$	$9.36\times10^{-32}(300/T_g)^{1.8}$	8
R15	$N+O_2(V1) \rightarrow O+NO$	$3.2\times10^{-12}(T_g/300)\exp(-(3150-2205.14)/T_g)$	9
R16	$N+O_2(V2) \rightarrow O+NO$	$3.2\times10^{-12}(T_g/300)\exp(-(3150-4410.28)/T_g)$	9
R17	$N+O_2(V3) \rightarrow O+NO$	$3.2\times10^{-12}(T_g/300)\exp(-(3150-6615.42)/T_g)$	9
R18	$N+O_2(V4) \rightarrow O+NO$	$3.2\times10^{-12}(T_g/300)\exp(-(3150-8704.5)/T_g)$	9
R19	$O+N_{2(}V1) \rightarrow N+NO$	$3.0\times10^{-10}\exp(-(38370-3380)/T_g)$	9
R20	$O+N_2(V2) \rightarrow N+NO$	$3.0\times10^{-10}\exp(-(38370-6850)/T_g)$	9
R21	$O+N_2(V3) \rightarrow N+NO$	$3.0\times10^{-10}\exp(-(38370-10200)/T_g)$	9
R22	$O+N_2(V4) \rightarrow N+NO$	$3.0\times10^{-10}\exp(-(38370-13600)/T_g)$	9
R23	$O+N_2(V5) \rightarrow N+NO$	$3.0\times10^{-10}\exp(-(38370-17100)/T_g)$	9
R24	$O+N_2(V6) \rightarrow N+NO$	$3.0\times10^{-10}\exp(-(38370-20400)/T_g)$	9

R25	$O+N_2(V7)\rightarrow N+NO$	$3.0\times10^{-10}\exp(-(38370-23908)/T_g)$	9
R26	$O+N_2(V8)\rightarrow N+NO$	$3.0\times10^{-10}\exp(-(38370-27274)/T_g)$	9
R27	$O+NO\rightarrow N+O_2$	$7.5\times10^{-12}(T_g/300)\exp(-79500/T_g)$	8
R28	$NO+O_2\rightarrow O+NO_2$	$2.8\times10^{-12}\exp(-23400/T_g)$	8
R29	$NO_2+NO_2\rightarrow NO+O+NO_2$	$4.012\times10^{-5}(300/T_g)^2\exp(-36180/T_g)$	8
R30	$NO_3+N_2\rightarrow NO2+O+N_2$	$3.1\times10^{-5}(300/T_g)^2\exp(-25000/T_g)$	8
R31	$O+NO+N_2\rightarrow NO_2+N_2$	$1.2\times10^{-31}(300/T_g)^{1.8}$	8
R32	$O+NO+O_2\rightarrow NO_2+O_2$	$9.36\times10^{-32}(300/T_g)^{1.8}$	8
R33	$N+NO\rightarrow O+N_2$	$1.8\times10^{-11}(T_g/300)^{0.5}$	8
R34	$N_2+O_2\rightarrow O+N_2O$	$2.5\times10^{-10}(-50390/T_g)$	8
R35	$N_2O_5+M\rightarrow NO_2+NO_3+M$	$1\times10^{-3}(300/T_g)^{3.5}\exp(-11000/T_g)$	10
B36	$NO_2+NO_3+M\rightarrow N_2O_5+M$	$2.8\times10^{-29}(300/T_g)^{3.5}$	10
R37	$NO+NO_3+M\rightarrow N_2O_3+M$	$3.09\times10^{-34}(300/T_g)^{7.7}$	10

R38	$NO+NO_3 \rightarrow NO_2+NO_2$	$1.8\times10^{-11}\exp(110/T_g)$	10
R39	$N_2+O_2 \rightarrow O+N_2O$	$2.5\times10^{-10}\exp(-50390/T_g)$	8
R40	$NO+NO \rightarrow O+N_2O$	$2.2\times10^{-12}\exp(-32100/T_g)$	8
R41	$O+N_2+M \rightarrow N_2O+M$	$3.9\times10^{-35}\exp(-10400/T_g)$	8
R42	$N_2O+N_2 \rightarrow N_2+O+N_2$	$1.2\times10^{-8}(300/T_g)\exp(-29000/T_g)$	8

Reference:

[1] C. Lin, W. Li, H. Chen, J. Feng, M. Zhu, J. Shi, M. Li, B. Hou, Z. Wang, X. Chen, J. Liu, W. Yan. Two-Step Tandem Catalysis for High-Efficiency Ammonia Synthesis Via Nitrate Reduction on Anion-Intercalated CoNi LDH and Cu/Cu_2O. *Adv. Sci.* 2025, 12(26), 202502262. DOI: 10.1002/advs.202502262

[2] Y. Zhang, L. Pei, X. Xu, J. Xu, J. Shen, M. Ye. In-situ growth of self-assembled 3D Cu_2O@Cu foam with enhanced electrochemical properties. *Electrochim. Acta* 2016, 221, 56-61. DOI: 10.1016/j.electacta.2016.10.150

[3] J. Zhao, L. Liu, Y. Yang, Insights into Electrocatalytic Nitrate Reduction to Ammonia via Cu-Based Bimetallic Catalysts. *ACS Sustain. Chem. Eng.* 2023, 11(6), 2468-2475. DOI: 10.1021/acssuschemeng.2c06498

[4] V. Phelps, L. C. Pitchford. Anisotropic scattering of electrons by N_2 and its effect on electron-transport. *Phys. Rev. A* 1985, 31(5), 2932. DOI: 10.1103/PhysRevA.31.2932

[5] H. Tawara, T. Kato. Total and partial ionization cross sections of atoms and ions by electron impact. *Atom. Data Nucl. Data Tables* 1987, 36(2), 167-353. DOI: 10.1016/0092-640X(87)90014-3

[6] G. Hagelaar, L. C. Pitchford. Solving the Boltzmann equation to obtain electron transport coefficients and rate coefficients for fluid models. *Plasma Sources Sci. Technol.* 2005, 14(4), 722-733. DOI: 10.1088/0963-0252/14/4/011

[7] W. Wang, R. Snoeckx, X. Zhang, M. S. Cha, A. Bogaerts. Modeling Plasma-based CO_2 and CH_4 Conversion in Mixtures with N_2, O_2, and H_2O: The Bigger Plasma Chemistry Picture. *J. Phys. Chem. C* 2018, 122(16), 8704-8723. DOI: 10.1021/acs.jpcc.7b10619

[8] M. Capitell, C. M. Ferreira, B. F. Gordiets, A. I. Osipov, Plasma Kinetics in Atmospheric Gases, *Springer Berlin, Heidelberg,* 2000.

[9] A. Fridman, Plasma Chemistry: Frontmatter, *Cambridge University Press,* Cambridge, 2008.

[10] Y. Sakiyama, D. B. Graves, H. Chang, T. Shimizu, G. E. Morfill. Plasma chemistry model of surface microdischarge in humid air and dynamics of reactive neutral species. *J. Phys. D-Appl. Phys.* 2012, 45(42), 425201. DOI: 10.1088/0022-3727/45/42/425201